

Anisotropic surface state band splitting and low energy flat bands in 3d correlated topological Kondo insulator candidate $FeSb_2$

Ziling Cao(曹紫菱), Jie Pang(庞杰), Yu Xu(徐煜), Taimin Miao(苗泰民), Bo Liang(梁波), Wenpei Zhu(朱文培), Neng Cai(蔡能), Mingkai Xu(徐明楷), Jumin Shi(史聚民), Yingjie Shu(束英杰), Yiwen Chen(陈逸雯), Jiachen Wang(王佳琛), Shenjin Zhang(张申金), Fengfeng Zhang(张丰丰), Feng Yang(杨峰), Zhimin Wang(王志敏), Qinjun Peng(彭钦军), Zhihai Zhu(朱志海), Xintong Li(李昕彤), Hanqing Mao(毛寒青), Guodong Liu(刘国东), Zuyan Xu(许祖彦), Youguo Shi(石友国), Lin Zhao(赵林), X. J. Zhou(周兴江)

Citation: Chin. Phys. B. 35, 097901 (2026). DOI: 10.1088/1674-1056/ae6d9f |
CSTR: 32038.14.CPB.ae6d9f
http://cpb.iphy.ac.cn; http://iopscience.iop.org/cpb

What follows is a list of articles you may be interested in

Measurement of far-infrared surface phonon polaritons in AlN nanowires via electron microscope

Chao He(何超), Ze Hua(华泽), Peiyi He(何沛一), Ruishi Qi(亓瑞时), Yuehui Li(李跃辉), Ruiwen Shao(邵瑞文), Weikang Dong(董伟康), Ruochen Shi(时若晨), Yeliang Wang(王业亮), Peng Gao(高鹏)
Chin. Phys. B. 35, 037901 (2026). DOI: 10.1088/1674-1056/ae2a00 | CSTR: 32038.14.CPB.ae2a00

Determination of the surface states from the ultrafast electronic states in a thermoelectric material

Tongyao Wu(吴桐尧), Hongyuan Wang(王洪远), Yuanyuan Yang(杨媛媛), Shaofeng Duan(段绍峰), Chaozhi Huang(黄超之), Tianwei Tang(唐天威), Yanfeng Guo(郭艳峰), Weidong Luo(罗卫东), Wentao Zhang(张文涛)
Chin. Phys. B. 31, 027902 (2022). DOI: 10.1088/1674-1056/ac373c

High-resolution angle-resolved photoemission study of oxygen adsorbed Fe/MgO(001)

Mingtian Zheng, Eike F. Schwier, Hideaki Iwasawa, Kenya Shimada
Chin. Phys. B. 29, 067901 (2020). DOI: 10.1088/1674-1056/ab9196

RAPID COMMUNICATION

Anisotropic surface state band splitting and low energy flat bands in 3d correlated topological Kondo insulator candidate $FeSb_2$

Ziling Cao(曹紫菱)[1,2,†], Jie Pang(庞杰)[1,2,†], Yu Xu(徐煜)[1,†], Taimin Miao(苗泰民)[1,†], Bo Liang(梁波)[1,2], Wenpei Zhu(朱文培)[1,2], Neng Cai(蔡能)[1,2], Mingkai Xu(徐明楷)[1,2], Jumin Shi(史聚民)[1,2], Yingjie Shu(束英杰)[1,2], Yiwen Chen(陈逸雯)[1,2], Jiachen Wang(王佳琛)[1,2], Shenjin Zhang(张申金)[3], Fengfeng Zhang(张丰丰)[3], Feng Yang(杨峰)[3], Zhimin Wang(王志敏)[3], Qinjun Peng(彭钦军)[3], Zhihai Zhu(朱志海)[1,2], Xintong Li(李昕彤)[1,2], Hanqing Mao(毛寒青)[1,2], Guodong Liu(刘国东)[1,2], Zuyan Xu(许祖彦)[3], Youguo Shi(石友国)[1,2], Lin Zhao(赵林)[1,2,‡], and X. J. Zhou(周兴江)[1,2,§]

[1] *National Laboratory for Superconductivity, Beijing National Laboratory for Condensed Matter Physics, Institute of Physics, Chinese Academy of Sciences, Beijing* 100190, *China*

[2] *University of Chinese Academy of Sciences, Beijing* 100049, *China*

[3] *Technical Institute of Physics and Chemistry, Chinese Academy of Sciences, Beijing* 100190, *China*

(Received 9 May 2026; revised manuscript received 9 May 2026; accepted manuscript online 14 May 2026)

$FeSb_2$ is a correlated narrow-gap semiconductor that has often been discussed as a 3d-electron Kondo insulator candidate and exhibits a low-temperature resistance plateau with possible surface-dominated conduction. We carried out a systematic high-resolution laser-based angle-resolved photoemission spectroscopy (ARPES) study of $FeSb_2$ to investigate its electronic structure. The surface states around the zone center show clear anisotropic splitting. When the temperature is lowered into the resistance plateau regime (< 6 K), the surface states remain robust, but their photoemission peaks become much sharper and gain spectral weight. Two distinct flat-band-like features are observed at low energy. One is located at ~ 127 meV below the Fermi level, which exists only along a specific high-symmetry direction, while the other is located at ~ 70 meV below the Fermi level and is present along all the measured momentum cuts around the zone center. These results provide new information to understand the renormalization effects, the resistance plateau, and the topological nature of $FeSb_2$.

Keywords: $FeSb_2$, ARPES, electronic structure, Kondo insulator

PACS: 79.60.–i, 71.27.+a, 71.20.–b, 73.20.–r

DOI: 10.1088/1674-1056/ae6d9f **CSTR:** 32038.14.CPB.ae6d9f

1. Introduction

Topological Kondo insulators have emerged as an important platform for studying how strong electronic correlations reshape band topology. In canonical 4f-electron Kondo insulators, the coherent hybridization between localized f moments and itinerant conduction electrons opens a narrow gap at low temperature, while spin–orbit coupling and band inversion can give rise to metallic boundary states within the bulk gap.[1–4] This framework has motivated extensive studies of SmB_6, YbB_{12}, $Ce_3Bi_4Pt_3$, $U_3Bi_4Ni_3$ and related narrow-gap correlated insulators, where low-temperature resistance saturation is often interpreted as a signature of residual surface conduction short-circuiting an insulating bulk.[5–9] Nevertheless, even in the prototypical f-electron systems, the topological origin of the observed surface states remains under active debate, as surface polarity, reconstruction, disorder, and correlation-driven in-gap states can complicate a simple topological interpretation.[10–14]

$FeSb_2$ provides a particularly intriguing 3d-electron counterpart to this problem. As a narrow-gap correlated semiconductor, it exhibits several phenomenological similarities to canonical Kondo insulators, including activated transport, strong correlation effects, and a low-temperature resistance plateau.[15–18] These observations have motivated discussions of $FeSb_2$ as a d-electron Kondo-insulator candidate, yet its microscopic origin remains debated. Alternative scenarios based on itinerant narrow-gap band physics, defect-induced in-gap states, phonon-drag effects, and spin-state excitations have also been proposed.[19–22] In this context, the origin of the low-temperature resistance plateau is a central issue. Recent transport measurements have indicated that the plateau is associated with surface-dominated conduction on top of an increasingly insulating bulk.[23,24] Angle-resolved photoemission spectroscopy (ARPES) studies have directly revealed metallic surface states in $FeSb_2$.[18,25] However, whether these surface states are topologically nontrivial,

[†]These authors contributed equally to this work.

[‡]Corresponding author. E-mail: lzhao@iphy.ac.cn

[§]Corresponding author. E-mail: XJZhou@iphy.ac.cn

© 2026 Chinese Physical Society and IOP Publishing Ltd. All rights, including for text and data mining, AI training, and similar technologies, are reserved.

reconstruction-induced, disorder-related, or manifestations of a more general correlated surface electronic structure remains unresolved.[24,26] $FeSb_2$ therefore offers a timely platform for examining how narrow-gap correlation physics, surface metallicity, and possible topology are intertwined in a 3d-electron system.

Here we investigate the electronic structure of $FeSb_2$ by high-resolution laser-based ARPES. We show that the surface states exhibit clear anisotropic band splitting and sharp photoemission peaks emerging in the low-temperature plateau regime. In addition to the flat band at the binding energy of ~ 127 meV, we observed another new flat band at ~ 70 meV below the Fermi level. These results provide new information to understand the renormalization effects, the resistance plateau, and the topological nature of $FeSb_2$.

2. Experiment

High-quality single crystals of $FeSb_2$ were grown by an Sb self-flux method.[27] Residual Sb flux on the as-grown crystal surfaces was mechanically removed before crystallographic orientation. The crystal orientation was determined by back-reflection Laue diffraction. The oriented crystals were then cut using a diamond wire saw. The sample was characterized by magnetization and electrical resistance measurements (Fig. 1(c)). The magnetization was measured under an applied field of 100 Oe with the magnetic field perpendicular to the b axis. The resistance increases by approximately 5 orders of magnitude between 300 K and 2 K and develops a plateau below about 6 K, consistent with previous reports for high-quality $FeSb_2$ crystals.[23,28]

ARPES measurements were carried out using laser-based systems with a photon energy of $h\nu = 6.994$ eV, equipped with either a hemispherical DA30L analyzer (Scienta-Omicron) (Figs. 2, 3, 5 and 6) or an angle-resolved time-of-flight (ARToF) analyzer (Scienta-Omicron) (Fig. 4).[29,30] The energy resolution was set to ~ 1 meV, and the angular resolution is $\sim 0.2^\circ$ with zero sample bias. To expand the accessible momentum range, a sample-bias technique was employed during the measurements.[31] The ARPES measurements were performed under different polarization geometries by combining various light polarizations, analyzer-slit orientations and the sample orientations. The light polarization can vary between linear polarizations and circular polarizations. All samples were cleaved *in situ* at low temperature and measured under ultrahigh vacuum with a base pressure better than 5×10^{-11} mbar. The cleavage temperature was 1.5 K for the ARToF measurements and 16 K for the DA30L measurements. The Fermi level (E_F) was referenced by measuring a clean polycrystalline gold which was electrically connected to the sample.

3. Results and discussion

$FeSb_2$ crystallizes in the orthorhombic marcasite structure (space group *Pnnm*). As shown in Fig. 1(a), each Fe atom is surrounded by six nearest-neighbor Sb atoms, forming a distorted $FeSb_6$ octahedron, while neighboring octahedra share edges along the short c axis.[15,27] The lattice constants are $a \approx 5.82$ Å, $b \approx 6.52$ Å and $c \approx 3.19$ Å. The high-symmetry points of the corresponding bulk Brillouin zone and their projections onto the (010) surface Brillouin zone are indicated in Fig. 1(b).

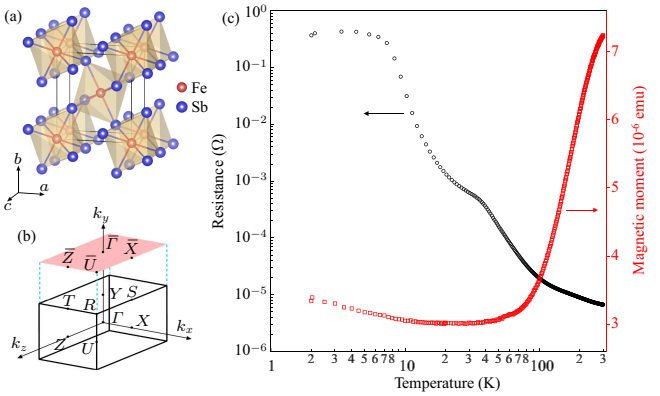


Fig. 1. Crystal structure, transport and magnetic properties of $FeSb_2$. (a) Crystal structure of $FeSb_2$, visualized using VESTA.[32] (b) First Brillouin zone of $FeSb_2$ and the projected surface Brillouin zone of the (010) surface, with the corresponding high-symmetry points indicated. (c) Temperature-dependent resistance (black curve) and magnetization (red curve) of $FeSb_2$. A pronounced resistance plateau is observed below ~ 6 K.

Figure 2 shows Fermi surface mappings of the cleaved $FeSb_2$(010) surface measured at 16 K under different measurement conditions. We first measured the work function of the cleaved surface by applying a sample bias; the work function was determined to be $\Phi = 4.781$ eV. Then the Fermi surface mappings were measured using different sample biases and different polarization geometries. The application of the sample bias allows us to cover a wider momentum range. When the sample bias is set to -99 V (Fig. 2(a)), the full 2π solid angle of photoelectrons can be collected, which gives the largest possible momentum coverage by the 6.994 eV laser excitation. Since the application of the sample bias deteriorates the momentum resolution, we also measured the Fermi surface with a lower sample bias of -49 V (Fig. 2(b)) and -20 V (Figs. 2(c)–2(e)). To make use of the photoemission matrix element effects, and in particular to reveal the orbital character of the observed Fermi surface, we also measured the Fermi surface mappings under different polarization geometries combining various light polarizations, analyzer-slit orientations, and the sample orientations.

From our Fermi surface measurements in Fig. 2, together with the band structure analysis in Fig. 3 and the previous ARPES studies,[18] we arrive at the measured Fermi surface topology of $FeSb_2$(010) shown in Fig. 2(f). It consists of two

small electron-like pockets around the zone center $\overline{\Gamma}$ (β_1 and β_2), an open Fermi surface along the $\overline{\Gamma}$–$\overline{X}$ direction (α), and a hole-like pocket around $\overline{Z}$ (γ). As the bulk $FeSb_2$ is a narrow-gap semiconductor, the observed Fermi surface features are all associated with surface-related states. When a large sample bias of −99 V is applied (Fig. 2a), in the accessible momentum space, the entire β pockets and part of the α and γ features are covered. But the observed β pockets are weak and broad in this case. When the sample bias is reduced to −49 V (Fig. 2(b)), the β pockets become slightly clearer but remain weak. Only when the sample bias is further reduced to −20 V (Figs. 2(c)–2(e)), the β pockets can still be fully covered and become much sharper and stronger under proper polarization geometries, like the second panel in Fig. 2(c).

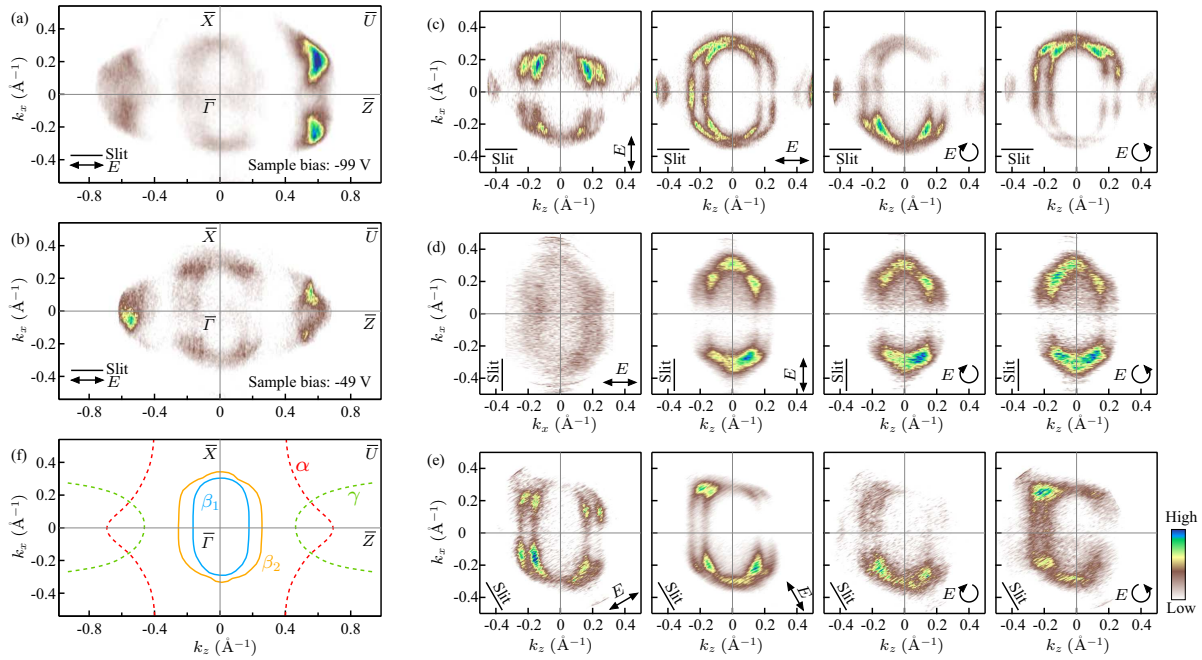


Fig. 2. Fermi surface mappings of $FeSb_2$ measured at 16 K under different sample bias voltages[31] and different polarization geometries. The analyzer slit orientation and the electric field, $\boldsymbol{E}$, of the laser light are indicated in each panel. (a) Fermi surface mapping of the $FeSb_2$ (010) surface measured under a sample bias voltage of −99 V. In this case, the full 2π solid angle of photoelectrons is collected. (b) Same as (a) but measured under a sample bias voltage of −49 V. (c)–(e) Fermi surface mappings measured under a sample bias voltage of −20 V with two linear polarizations and two circular polarizations for the slit direction along $\overline{\Gamma}$–$\overline{Z}$ (c), $\overline{\Gamma}$–$\overline{X}$ (d) and $\overline{\Gamma}$–$\overline{U}$ (e), respectively. (f) Fermi surface of $FeSb_2$ extracted from experimental data, including two surface-state sheets β_1 and β_2 and the α and γ sheets reported in Ref. [18].

The β pockets around $\overline{\Gamma}$ show a clear splitting into two branches, which we label β_1 and β_2 in Fig. 2(f). The observed splitting is anisotropic in momentum space. The splitting is strongest along the $\overline{\Gamma}$–$\overline{Z}$ direction, but it is weakest along the $\overline{\Gamma}$–$\overline{X}$ direction. The splitting variation can also be clearly seen in the corresponding momentum dependent band structures shown in Fig. 3(a). We find that, while the splitting is smallest along $\overline{\Gamma}$–$\overline{X}$, there is still a clear splitting between β_1 and β_2 along this direction, which is most clearly revealed in the band structure measured along the $\overline{\Gamma}$–$\overline{X}$ direction (last panel in Fig. 3(a)). Our high-resolution laser ARPES measurements thus provide a slightly different picture of the β pockets compared with the previous ARPES studies where the β band splitting was not clearly resolved along the $\overline{\Gamma}$–$\overline{X}$ direction.[18]

Figure 3(a) shows the band structures along a series of momentum cuts centered around $\overline{\Gamma}$, measured under the optimal geometry for resolving the β pockets. The corresponding momentum locations of the cuts are indicated in Fig. 3(b). The splitting of the β band into β_1 and β_2 is clearly resolved along all the cuts, with the strongest splitting along cut 1 parallel to $\overline{\Gamma}$–$\overline{Z}$ and the weakest splitting along cut 7 parallel to $\overline{\Gamma}$–$\overline{X}$. The Fermi velocity of both β_1 and β_2 bands is similar, which is ~ 0.53 eV·Å along $\overline{\Gamma}$–$\overline{Z}$ (first panel in Fig. 3(a)) and ~ 0.28 eV·Å along $\overline{\Gamma}$–$\overline{X}$ (last panel in Fig. 3(a)). Considering the Fermi momentum of the two bands, this gives an effective mass of about 2.5 m_e for β_1 and 3.8 m_e for β_2 along $\overline{\Gamma}$–$\overline{Z}$, and about 8.0 m_e for β_1 and 9.1 m_e for β_2 along $\overline{\Gamma}$–$\overline{X}$. Figure 3(c) shows the stacked energy distribution curves (EDCs) for cut 1. At 16 K, the γ, β_1 and β_2 bands all develop well-defined peaks near E_F in spite of their relatively weak spectral weight. The width of the β_1 and β_2 peaks is about 10 meV.

To further examine the electronic structure of $FeSb_2$ in the low-temperature plateau regime, we performed laser ARPES measurements at 1.5 K. The measured Fermi surface mapping is shown in Fig. 4(a), while Fig. 4(b) shows the band structure measured along a momentum cut parallel to $\overline{\Gamma}$–$\overline{Z}$ (cut 1). The associated stacked EDCs are presented in Fig. 4(c). Overall, the electronic structure at 1.5 K is qualitatively similar to that measured at 16 K. The two surface bands, β_1 and β_2, remain clearly visible around $\overline{\Gamma}$ and preserve the same split structure observed at higher temperature. Their spectral weight, however, is substantially enhanced at 1.5 K. In the stacked

EDCs for cut 1 (Fig. 4(c)), the corresponding peaks become markedly sharper and stronger near E_F. To examine this behavior more systematically, we extracted a series of EDCs at the k_F points on the β_2 (Fig. 4(d)) and β_1 (Fig. 4(e)) pockets. Although the peak intensities vary from point to point because of the matrix element effects, the peaks are consistently much narrower at 1.5 K, with a width of about 7.1 meV. Despite the pronounced low-temperature sharpening and spectral-weight enhancement, no clear gap opening is resolved near the peak positions. Within the momentum region around $\overline{\Gamma}$ probed here, cooling into the low-temperature plateau regime is therefore not accompanied by an obvious band reconstruction or any similarly abrupt change in the electronic structure. Instead, the observed evolution is more consistent with enhanced coherence of pre-existing states rather than a low-temperature electronic phase transition.[14,24]

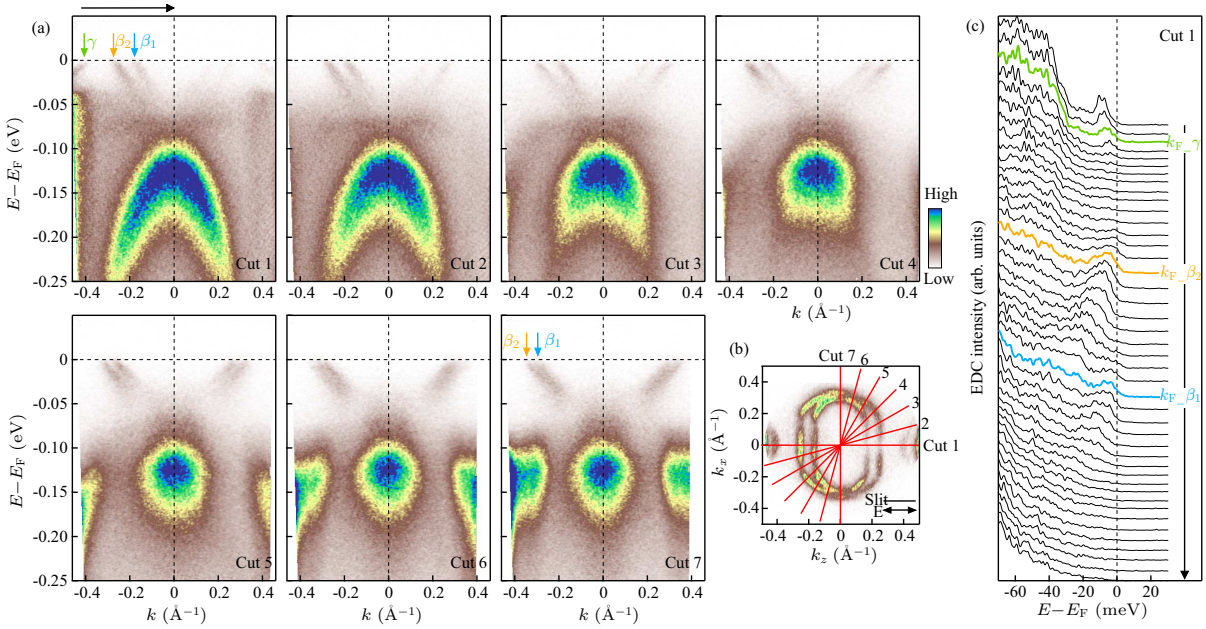


Fig. 3. Detailed band structures of the β_1 and β_2 bands around $\overline{\Gamma}$ measured at 16 K under the sample bias voltage of −20 V with the polarization geometry the same as in the second panel of Fig. 2(c). (a) Band structures measured along a series of momentum cuts centered around $\overline{\Gamma}$. The corresponding cut locations (cuts 1–7) are marked by red lines in (b). (b) Fermi surface mapping of $FeSb_2$ with the momentum cuts marked. (c) Stacked EDCs obtained from the first panel of (a) measured along the momentum cut 1 which is along the $\overline{\Gamma}$–$\overline{Z}$ direction.

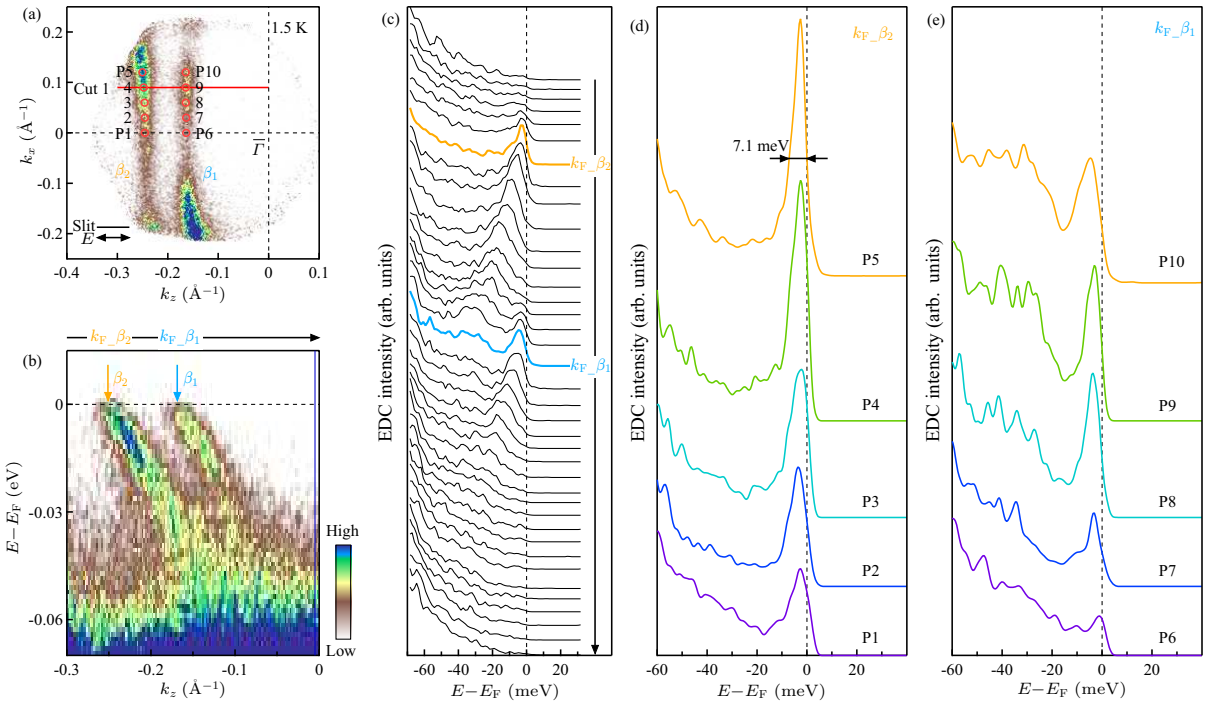


Fig. 4. Electronic structure of the β_1 and β_2 bands measured at 1.5 K. (a) Fermi surface mapping of $FeSb_2$ focusing on the β_1 and β_2 sheets. (b) Band structure along the momentum cut 1 marked by the red line in (a). (c) Stacked EDCs obtained from (b). (d) EDCs along the β_2 Fermi surface. The corresponding k_F points (P1–P5) are marked by red circles in (a). For clarity, the EDCs are offset along the vertical axis. (e) Same as (d) but for the β_1 Fermi surface, with the k_F points (P6–P10) marked by red circles in (a).

Now we turn to the low-energy flat bands observed in $FeSb_2$. Figure 5(a) shows a clear observation of a weakly dispersive feature, labeled FB1, at ~ 127 meV below E_F in the band structure measured along the $\overline{\Gamma}$–$\overline{X}$ direction. This FB1 band exhibits a pronounced matrix-element dependence and is observed most clearly under the measurement geometry indicated in the inset of Fig. 5(b). The feature becomes more pronounced in the EDC second derivative image shown in Fig. 5(b). Figure 5(c) shows the stacked EDCs for the same cut, where the FB1 feature is resolved as a clear peak at ~ 127 meV below E_F. Within the measured momentum range, the energy position of FB1 varies by no more than 6 meV, indicating a weakly dispersive character. We note that the EDC peaks are broad, which is ~ 100 meV in width. The energy position of this FB1 feature and its weakly dispersive character closely resemble those of the strongly renormalized band reported in previous ARPES and dynamical mean-field theory (DMFT) studies.[18,25]

To study the momentum dependence of FB1, we measured band structures along a series of momentum cuts centered around $\overline{\Gamma}$, as shown in Fig. 5(d). As shown in the second derivative image in Fig. 5(a) and the first panel in Fig. 5(d), the FB1 feature appears to be composed of three sub-features, one central feature FB1a and two side features FB1b and FB1c. When the momentum cut is slightly rotated away from the $\overline{\Gamma}$–$\overline{X}$ direction (second panel in Fig. 5(d) for cut 2), the FB1a feature remains at essentially the same energy, while the FB1b and FB1c features show a clear dispersion. When the momentum cuts are further rotated (third to seventh panels in Fig. 5(d) for cut 3 to cut 7), the FB1b and FB1c features disappear in the covered momentum region. These results indicate that the overall flat-band-like FB1 feature exists over a narrow momentum region around $\overline{\Gamma}$–$\overline{X}$ direction.

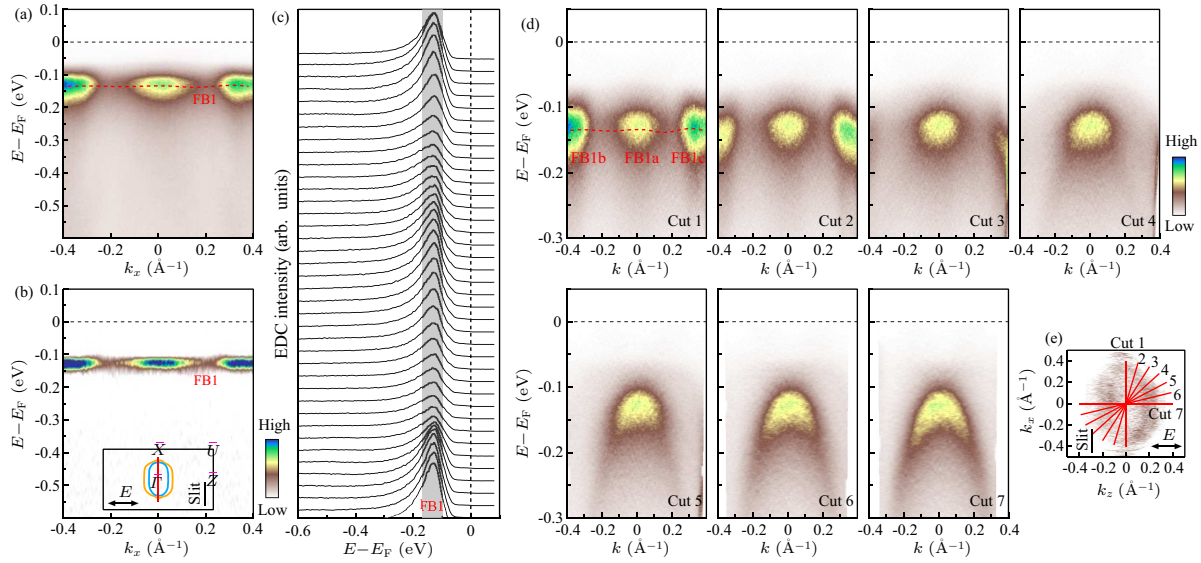


Fig. 5. Observation of a flat band FB1 at a binding energy of ~ 127 meV and its momentum dependence. (a) Band structure measured along the $\overline{\Gamma}$–$\overline{X}$ direction, showing a flat-band feature (FB1) at about 127 meV below E_F. (b) EDC second derivative of (a). The measurement geometry and the location of the momentum cut (red line) are shown in the inset. (c) Stacked EDCs obtained from (a) where the flat band FB1 features are highlighted. (d) Band structures measured along a series of momentum cuts centered around $\overline{\Gamma}$. The corresponding cut locations (cuts 1–7) are marked by red lines in (e). (e) Fermi surface mapping of $FeSb_2$ with the momentum cuts marked.

Figure 6 shows the first observation of another flat-band-like feature, labeled FB2, at ~ 70 meV below E_F. Figure 6(a) presents the band structure measured along the $\overline{\Gamma}$–$\overline{Z}$ direction. A flat-band-like feature is clearly observed at ~ 70 meV below E_F, labeled as FB2. This FB2 feature is more clearly revealed in the EDC second derivative image shown in Fig. 6(b). Figure 6(c) shows the stacked EDCs for the same cut, where the FB2 feature is resolved as a clear peak at ~ 70 meV below E_F. The FB2 feature exists within a finite momentum range between $[-0.33, 0.33]$ Å^{-1} along $\overline{\Gamma}$–$\overline{Z}$. Within the momentum range, the energy position of FB2 varies by no more than 5 meV, indicating an extremely weak dispersion. Different from the FB1 feature, the EDC peaks of FB2 are sharp, with a width of about 15 meV.

Figures 6(d)–6(f) show the band structure, EDC second derivative image and stacked EDCs for a cut along the $\overline{\Gamma}$–$\overline{X}$ direction. The FB2 flat band feature is also clearly observed along this direction at the same energy position of ~ 70 meV below E_F. The momentum range of FB2 along $\overline{\Gamma}$–$\overline{X}$ is about $[-0.13, 0.13]$ Å^{-1}. Different from the FB1 feature, the FB2 flat band feature is present along all the momentum cuts around the $\overline{\Gamma}$ point.

An important question raised by the present results is about the origin of the observed surface states and their relation to the low-temperature resistance plateau. So far, there have been no band structure calculations that can fully capture the observed surface states.[17,25] The topological nature of the observed surface states also needs further investigation. A re-

lated question concerns how the resistance plateau is reflected in the low-energy states observed by ARPES. As shown in Fig. 4, within the momentum window around $\overline{\Gamma}$, cooling into the plateau regime does not induce an abrupt band reconstruction, a clear gap opening, or a distinct new in-gap feature. Instead, the dominant changes are a sharpening of the pre-existing β branches and an enhancement of their spectral weight. This behavior shows that the plateau regime is associated with the low-temperature strengthening of pre-existing states, rather than with a sudden electronic reconstruction.

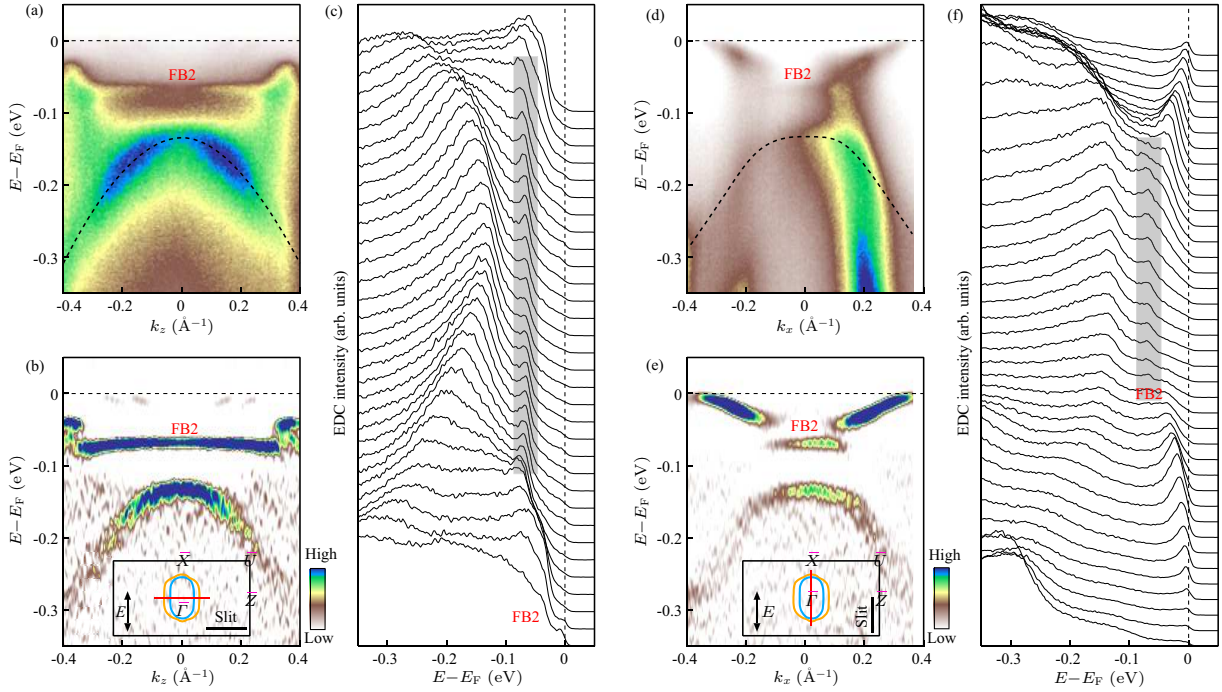


Fig. 6. Observation of a flat band FB2 at a binding energy of $\sim$ 70 meV. (a) Band structure measured along the $\overline{\Gamma}$–$\overline{Z}$ direction, showing a flat-band feature (FB2) at about 70 meV below E_F. The bulk band is indicated by the black dashed line. (b) EDC second derivative of (a). The measurement geometry and the location of the momentum cut (red line) are shown in the inset. (c) Stacked EDCs obtained from (a) where the flat band FB2 features are highlighted. (d)–(f) Same as (a)–(c) but measured along the $\overline{\Gamma}$–$\overline{X}$ direction and under the polarization geometry as marked in the inset of (e).

4. Summary

High-resolution laser-based ARPES measurements were carried out on $FeSb_2$. The surface states around $\overline{\Gamma}$ exhibit clear anisotropic band splitting. When the sample is cooled down into the low-temperature plateau regime, the surface states remain robust, but their photoemission peaks become much sharper and gain spectral weight. We observed two distinct flat-band-like features at low energy. One is located at $\sim$ 127 meV below the Fermi level, which exists only along $\overline{\Gamma}$–$\overline{X}$, while the other is located at $\sim$ 70 meV below the Fermi level and is present along all the measured momentum cuts around $\overline{\Gamma}$. The present results support a multicomponent picture of $FeSb_2$, with surface β branches, flat low-energy features, and correlation-driven renormalization contributing to the plateau-regime electronic structure. Because the present ARPES data mainly probe the vicinity of $\overline{\Gamma}$, more subtle low-temperature changes elsewhere in the surface Brillouin zone, such as near $\overline{Z}$ or $\overline{U}$, cannot be excluded. ARPES spectral weight alone also cannot determine the contribution of the surface-related channel to the total electrical conduction. Further progress will require wider momentum-space mapping, spin-resolved ARPES, and more theoretical efforts.

Acknowledgements

This work is supported by the National Key Research and Development Program of China (Grant Nos. 2024YFA1408301, 2021YFA1401800, 2022YFA1604200, 2022YFA1403900, 2023YFA1406002, 2023YFA1406103, and 2024YFA1408100), the National Natural Science Foundation of China (Grant Nos. 12488201, 12374066, 12374154, and 12494593), CAS Superconducting Research Project (Grant No. SCZX-0101), Quantum Science and Technology National Science and Technology Major Project of China (Grant No. 2021ZD0301800), and Synergetic Extreme Condition User Facility (SECUF).

References

[1] Dzero M, Sun K, Galitski V and Coleman P 2010 *Phys. Rev. Lett.* **104** 106408

[2] Fisk Z, Sarrao J L, Cooper S L, Nyhus P, Boebinger G S, Passner A and Canfield P C 1996 *Physica B* **223–224** 409

[3] Lu F, Zhao J, Weng H, Fang Z and Dai X 2013 *Phys. Rev. Lett.* **110** 096401

[4] Dzero M, Xia J, Galitski V and Coleman P 2016 *Annu. Rev. Condens. Matter Phys.* **7** 249

[5] Wolgast S, Kurdak Ç, Sun K, Allen J W, Kim D J and Fisk Z 2013 *Phys. Rev. B* **88** 180405

[6] Kim D J, Thomas S, Grant T, Botimer J, Fisk Z and Xia J 2013 *Sci. Rep.* **3** 3150

[7] Sato Y, Xiang Z, Kasahara Y, Kasahara S, Chen L, Tinsman C, Iga F, Singleton J, Nair N L, Maksimovic N, Analytis J G, Li L and Matsuda Y 2021 *J. Phys. D: Appl. Phys.* **54** 404002

[8] Wakeham N, Rosa P F S, Wang Y Q, Kang M, Fisk Z, Ronning F and Thompson J D 2016 *Phys. Rev. B* **94** 035127

[9] Broyles C, Wan X, Cheng W, Wu D, Tan H, Xu Q, Gould S L, Siddiquee H, Xiao L, Chen R, Lin W, Wu Y, Regmi P, Eo Y S, Liu J, Chen Y, Yan B, Sun K and Ran S 2025 *Sci. Adv.* **11** eadq9952

[10] Xu N, Biswas P K, Dil J H, Dhaka R S, Landolt G, Muff S, Matt C E, Shi X, Plumb N C, Radović M, Pomjakushina E, Conder K, Amato A, Borisenko S V, Yu R, Weng H M, Fang Z, Dai X, Mesot J, Ding H and Shi M 2014 *Nat. Commun.* **5** 4566

[11] Hlawenka P, Siemensmeyer K, Weschke E, Varykhalov A, Sánchez-Barriga J, Shitsevalova N Y, Dukhnenko A V, Filipov V B, Gabáni S, Flachbart K, Rader O and Rienks E D L 2018 *Nat. Commun.* **9** 517

[12] Ohtsubo Y, Yamashita Y, Hagiwara K, Ideta S, Tanaka K, Yukawa R, Horiba K, Kumigashira H, Miyamoto K, Okuda T, Hirano W, Iga F and Kimura S 2019 *Nat. Commun.* **10** 2298

[13] Hagiwara K, Ohtsubo Y, Matsunami M, Ideta S, Tanaka K, Miyazaki H, Rault J E, Le Fèvre P, Bertran F, Taleb-Ibrahimi A, Yukawa R, Kobayashi M, Horiba K, Kumigashira H, Sumida K, Okuda T, Iga F and Kimura S 2016 *Nat. Commun.* **7** 12690

[14] Pickem M, Maggio E and Tomczak J M 2021 *Commun. Phys.* **4** 226

[15] Petrovic C, Lee Y, Vogt T, Lazarov N Dj, Bud'ko S L and Canfield P C 2005 *Phys. Rev. B* **72** 045103

[16] Takahashi H, Okazaki R, Yasui Y and Terasaki I 2011 *Phys. Rev. B* **84** 205215

[17] Homes C C, Du Q, Petrovic C, Brito W H, Choi S and Kotliar G 2018 *Sci. Rep.* **8** 11692

[18] Xu K J, Chen S D, He Y, He J, Tang S, Jia C, Ma E Y, Mo S K, Lu D, Hashimoto M, Devereaux T P and Shen Z X 2020 *Proc. Natl. Acad. Sci. USA* **117** 15409

[19] Diakhate M S, Hermann R P, Möchel A, Sergueev I, Søndergaard M, Christensen M and Verstraete M J 2011 *Phys. Rev. B* **84** 125210

[20] Battiato M, Tomczak J M, Zhong Z and Held K 2015 *Phys. Rev. Lett.* **114** 236603

[21] Du Q, Wu L, Cao H, Kang C J, Nelson C, Pascut G L, Besara T, Siegrist T, Haule K, Kotliar G, Zaliznyak I, Zhu Y and Petrovic C 2021 *npj Quantum Mater.* **6** 13

[22] Li H, Wang G, Ding N, Ren Q, Zhao G, Lin W, Yang J, Yan W, Li Q, Yang R, Yuan S, Denlinger J D, Wang Z, Zhang X, Wray L A, Dong S, Qian D and Miao L 2024 *Proc. Natl. Acad. Sci. USA* **121** e2321193121

[23] Eo Y S, Avers K, Horn J A, Yoon H, Saha S R, Suarez A, Fuhrer M S and Paglione J 2023 *Appl. Phys. Lett.* **122** 233102

[24] Eaton A G, Popiel N J M, Xu K J, Hickey A J, Liu H, Ciomaga Hatnean M, Balakrishnan G, Lange G F, Slager R J, Shen Z X and Sebastian S E 2024 arXiv 2403.04550

[25] Chikina A, Ma J Z, Brito W H, Choi S, Sémon P, Kutepov A, Du Q, Jandke J, Liu H, Plumb N C, Shi M, Petrovic C, Radovic M and Kotliar G 2020 *Phys. Rev. Res.* **2** 023190

[26] Horn J A, Eo Y S, Avers K, Yoon H, Dorman R G, Saha S R and Paglione J 2026 *Phys. Rev. B* **113** 125142

[27] Petrovic C, Kim J W, Bud'ko S L, Goldman A I, Canfield P C, Choe W and Miller G J 2003 *Phys. Rev. B* **67** 155205

[28] Sun P, Oeschler N, Johnsen S, Iversen B B and Steglich F 2010 *Dalton Trans.* **39** 1012

[29] Liu G, Wang G, Zhu Y, Zhang H, Zhang G, Wang X, Zhou Y, Zhang W, Liu H, Zhao L, Meng J, Dong X, Chen C, Xu Z and Zhou X J 2008 *Rev. Sci. Instrum.* **79** 023105

[30] Zhou X, He S, Liu G, Zhao L, Yu L and Zhang W 2018 *Rep. Prog. Phys.* **81** 062101

[31] Miao T, Xu Y, Liang B, Zhu W, Cai N, Xu M, Wu D, Gu H, Mao W, Zhang S, Zhang F, Yang F, Wang Z, Peng Q, Xu Z, Zhu Z, Li X, Mao H, Zhao L, Liu G and Zhou X J 2026 *Rev. Sci. Instrum.* **97** 033908

[32] Momma K and Izumi F 2011 *J. Appl. Crystallogr.* **44** 1272